

## PDF hosted at the Radboud Repository of the Radboud University Nijmegen

The following full text is a publisher's version.

For additional information about this publication click this link.

<http://hdl.handle.net/2066/124449>

Please be advised that this information was generated on 2017-12-05 and may be subject to change.

## Measurement of the $\tau$ topological branching ratios at LEP

OPAL Collaboration

P.D. Acton<sup>a</sup>, G. Alexander<sup>b</sup>, J. Allison<sup>c</sup>, P.P. Allport<sup>d</sup>, K.J. Anderson<sup>e</sup>, S. Arcelli<sup>f</sup>,  
A. Astbury<sup>g</sup>, D. Axen<sup>h</sup>, G. Azuelos<sup>i,1</sup>, G.A. Bahan<sup>c</sup>, J.T.M. Baines<sup>c</sup>, A.H. Ball<sup>j</sup>, J. Banks<sup>c</sup>,  
G.J. Barker<sup>k</sup>, R.J. Barlow<sup>c</sup>, S. Barnett<sup>c</sup>, J.R. Batley<sup>d</sup>, G. Beaudoin<sup>i</sup>, A. Beck<sup>b</sup>, J. Becker<sup>l</sup>,  
T. Behnke<sup>m</sup>, K.W. Bell<sup>n</sup>, G. Bella<sup>b</sup>, P. Berlich<sup>l</sup>, S. Bethke<sup>o</sup>, O. Biebel<sup>p</sup>, U. Binder<sup>l</sup>,  
I.J. Bloodworth<sup>q</sup>, P. Bock<sup>o</sup>, B. Boden<sup>p</sup>, H.M. Bosch<sup>o</sup>, S. Bougerolle<sup>h</sup>, H. Breuker<sup>r</sup>,  
R.M. Brown<sup>n</sup>, R. Brun<sup>r</sup>, A. Buijs<sup>r</sup>, H.J. Burckhart<sup>r</sup>, P. Capiluppi<sup>f</sup>, R.K. Carnegie<sup>s</sup>,  
A.A. Carter<sup>k</sup>, J.R. Carter<sup>d</sup>, C.Y. Chang<sup>j</sup>, D.G. Charlton<sup>r</sup>, P.E.L. Clarke<sup>a</sup>, I. Cohen<sup>b</sup>,  
W.J. Collins<sup>d</sup>, J.E. Conboy<sup>t</sup>, M. Cooper<sup>u</sup>, M. Couch<sup>q</sup>, M. Coupland<sup>v</sup>, M. Cuffiani<sup>f</sup>, S. Dado<sup>u</sup>,  
G.M. Dallavalle<sup>f</sup>, S. De Jong<sup>r</sup>, L.A. del Pozo<sup>d</sup>, M.M. Deninno<sup>f</sup>, A. Dieckmann<sup>o</sup>, M. Dittmar<sup>w</sup>,  
M.S. Dixit<sup>x</sup>, E. do Couto e Silva<sup>y</sup>, J.E. Duboscq<sup>r</sup>, E. Duchovni<sup>z</sup>, G. Duckeck<sup>o</sup>, I.P. Duerdoth<sup>c</sup>,  
D.J.P. Dumas<sup>s</sup>, P.A. Elcombe<sup>d</sup>, P.G. Estabrooks<sup>s</sup>, E. Etzion<sup>b</sup>, H.G. Evans<sup>e</sup>, F. Fabbri<sup>f</sup>,  
M. Fincke-Keeler<sup>g</sup>, H.M. Fischer<sup>p</sup>, D.G. Fong<sup>j</sup>, C. Fukunaga<sup>aa,2</sup>, A. Gaidot<sup>ab</sup>, O. Ganel<sup>z</sup>,  
J.W. Gary<sup>w</sup>, J. Gascon<sup>i</sup>, R.F. McGowan<sup>c</sup>, N.I. Geddes<sup>n</sup>, C. Geich-Gimbel<sup>p</sup>, S.W. Gensler<sup>e</sup>,  
F.X. Gentit<sup>ab</sup>, G. Giacomelli<sup>f</sup>, V. Gibson<sup>d</sup>, W.R. Gibson<sup>k</sup>, J.D. Gillies<sup>n</sup>, J. Goldberg<sup>u</sup>,  
M.J. Goodrick<sup>d</sup>, W. Gorn<sup>w</sup>, C. Grandi<sup>f</sup>, F.C. Grant<sup>d</sup>, J. Hagemann<sup>m</sup>, G.G. Hanson<sup>y</sup>,  
M. Hansroul<sup>r</sup>, C.K. Hargrove<sup>x</sup>, P.F. Harrison<sup>k</sup>, J. Hart<sup>r</sup>, P.M. Hattersley<sup>q</sup>, M. Hauschild<sup>r</sup>,  
C.M. Hawkes<sup>r</sup>, E. Heflin<sup>w</sup>, R.J. Hemingway<sup>s</sup>, R.D. Heuer<sup>r</sup>, J.C. Hill<sup>d</sup>, S.J. Hillier<sup>q</sup>,  
D.A. Hinshaw<sup>i</sup>, J.D. Hobbs<sup>r</sup>, P.R. Hobson<sup>a</sup>, D. Hochman<sup>z</sup>, R.J. Homer<sup>q</sup>, A.K. Honma<sup>g,1</sup>,  
S.R. Hou<sup>j</sup>, C.P. Howarth<sup>t</sup>, R.E. Hughes-Jones<sup>c</sup>, R. Humbert<sup>l</sup>, P. Igo-Kemenes<sup>o</sup>, H. Ihssen<sup>o</sup>,  
D.C. Imrie<sup>a</sup>, A.C. Janissen<sup>s</sup>, A. Jawahery<sup>j</sup>, P.W. Jeffreys<sup>n</sup>, H. Jeremie<sup>i</sup>, M. Jimack<sup>f</sup>, M. Jobes<sup>q</sup>,  
R.W.L. Jones<sup>k</sup>, P. Jovanovic<sup>q</sup>, D. Karlen<sup>s</sup>, K. Kawagoe<sup>aa</sup>, T. Kawamoto<sup>aa</sup>, R.K. Keeler<sup>g</sup>,  
R.G. Kellogg<sup>j</sup>, B.W. Kennedy<sup>t</sup>, D.E. Klem<sup>x</sup>, T. Kobayashi<sup>aa</sup>, T.P. Kokott<sup>p</sup>, S. Komamiya<sup>aa</sup>,  
L. Köpke<sup>r</sup>, J.F. Kral<sup>r</sup>, R. Kowalewski<sup>s</sup>, J. von Krogh<sup>o</sup>, J. Kroll<sup>e</sup>, M. Kuwano<sup>aa</sup>, P. Kyberd<sup>k</sup>,  
G.D. Lafferty<sup>c</sup>, F. Lamarche<sup>i</sup>, J.G. Layter<sup>w</sup>, P. Le Du<sup>ab</sup>, P. Leblanc<sup>i</sup>, A.M. Lee<sup>j</sup>, M.H. Lehto<sup>t</sup>,  
D. Lellouch<sup>z</sup>, P. Lennert<sup>o</sup>, C. Leroy<sup>i</sup>, J. Letts<sup>w</sup>, S. Levegrün<sup>p</sup>, L. Levinson<sup>z</sup>, S.L. Lloyd<sup>k</sup>,  
F.K. Loebinger<sup>c</sup>, J.M. Lorah<sup>j</sup>, B. Lorazo<sup>i</sup>, M.J. Losty<sup>x</sup>, X.C. Lou<sup>y</sup>, J. Ludwig<sup>l</sup>, M. Mannelli<sup>r</sup>,  
S. Marcellini<sup>f</sup>, G. Maringer<sup>p</sup>, A.J. Martin<sup>k</sup>, J.P. Martin<sup>i</sup>, T. Mashimo<sup>aa</sup>, P. Mättig<sup>p</sup>, U. Maur<sup>p</sup>,  
J. McKenna<sup>g</sup>, T.J. McMahon<sup>q</sup>, J.R. McNutt<sup>a</sup>, F. Meijers<sup>r</sup>, D. Menszner<sup>o</sup>, F.S. Merritt<sup>e</sup>,  
H. Mes<sup>x</sup>, A. Michelini<sup>r</sup>, R.P. Middleton<sup>n</sup>, G. Mikenberg<sup>z</sup>, J. Mildenerberger<sup>s</sup>, D.J. Miller<sup>t</sup>,  
C. Milstene<sup>f,3</sup>, R. Mir<sup>y</sup>, W. Mohr<sup>l</sup>, C. Moisan<sup>i</sup>, A. Montanari<sup>f</sup>, T. Mori<sup>aa</sup>, T. Mouthuy<sup>y,4</sup>,  
B. Nellen<sup>p</sup>, H.H. Nguyen<sup>e</sup>, S.W. O'Neale<sup>r,5</sup>, F.G. Oakham<sup>x</sup>, F. Odorici<sup>f</sup>, M. Ogg<sup>s</sup>,  
H.O. Ogren<sup>y</sup>, H. Oh<sup>w</sup>, C.J. Oram<sup>g,1</sup>, M.J. Oreglia<sup>e</sup>, S. Orito<sup>aa</sup>, J.P. Pansart<sup>ab</sup>,  
B. Panzer-Steindel<sup>r</sup>, P. Paschievici<sup>z</sup>, G.N. Patrick<sup>n</sup>, N. Paz-Jaoshvili<sup>b</sup>, P. Pfister<sup>l</sup>,  
J.E. Pilcher<sup>e</sup>, D. Pitman<sup>g</sup>, D.E. Plane<sup>r</sup>, P. Poffenberger<sup>g</sup>, B. Poli<sup>f</sup>, A. Pouladdej<sup>s</sup>, E. Prebys<sup>r</sup>,  
T.W. Pritchard<sup>k</sup>, H. Przysiezniak<sup>i</sup>, G. Quast<sup>m</sup>, M.W. Redmond<sup>e</sup>, D.L. Rees<sup>q</sup>, G.E. Richards<sup>c</sup>,  
K. Riles<sup>w</sup>, S.A. Robins<sup>k</sup>, D. Robinson<sup>r</sup>, A. Rollnik<sup>p</sup>, J.M. Roney<sup>e</sup>, E. Ros<sup>r</sup>, S. Rossberg<sup>l</sup>,  
A.M. Rossi<sup>f,6</sup>, M. Rosvick<sup>g</sup>, P. Routenburg<sup>s</sup>, K. Runge<sup>l</sup>, O. Runolfsson<sup>r</sup>, D.R. Rust<sup>y</sup>,  
S. Sanghera<sup>s</sup>, M. Sasaki<sup>aa</sup>, C. Sbarra<sup>r</sup>, A.D. Schaile<sup>l</sup>, O. Schaile<sup>l</sup>, W. Schappert<sup>s</sup>,  
P. Scharff-Hansen<sup>r</sup>, P. Schenk<sup>g</sup>, H. von der Schmitt<sup>o</sup>, S. Schreiber<sup>p</sup>, C. Schwick<sup>m</sup>,

J. Schwiening<sup>p</sup>, W.G. Scott<sup>n</sup>, M. Settles<sup>y</sup>, B.C. Shen<sup>w</sup>, P. Sherwood<sup>t</sup>, R. Shypit<sup>h</sup>, A. Simon<sup>p</sup>, P. Singh<sup>k</sup>, G.P. Siropi<sup>f</sup>, A. Skuja<sup>j</sup>, A.M. Smith<sup>r</sup>, T.J. Smith<sup>r</sup>, G.A. Snow<sup>j</sup>, R. Sobie<sup>g,7</sup>, R.W. Springer<sup>j</sup>, M. Sproston<sup>n</sup>, K. Stephens<sup>c</sup>, J. Steuerer<sup>g</sup>, R. Ströhmer<sup>o</sup>, D. Strom<sup>e,8</sup>, H. Takeda<sup>aa</sup>, T. Takeshita<sup>aa,9</sup>, P. Taras<sup>i</sup>, S. Tarem<sup>z</sup>, P. Teixeira-Dias<sup>o</sup>, N. Tesch<sup>p</sup>, N.J. Thackray<sup>q</sup>, G. Transtromer<sup>a</sup>, N.J. Tresilian<sup>c</sup>, T. Tsukamoto<sup>aa</sup>, M.F. Turner<sup>d</sup>, G. Tysarczyk-Niemeyer<sup>o</sup>, D. Van den plas<sup>i</sup>, R. Van Kooten<sup>r</sup>, G.J. VanDalen<sup>w</sup>, G. Vasseur<sup>ab</sup>, C.J. Virtue<sup>x</sup>, A. Wagner<sup>m</sup>, D.L. Wagner<sup>e</sup>, C. Wahl<sup>l</sup>, J.P. Walker<sup>q</sup>, C.P. Ward<sup>d</sup>, D.R. Ward<sup>d</sup>, P.M. Watkins<sup>q</sup>, A.T. Watson<sup>q</sup>, N.K. Watson<sup>r</sup>, M. Weber<sup>o</sup>, P. Weber<sup>s</sup>, S. Weisz<sup>r</sup>, P.S. Wells<sup>r</sup>, N. Wermes<sup>o</sup>, M.A. Whalley<sup>q</sup>, G.W. Wilson<sup>ab</sup>, J.A. Wilson<sup>q</sup>, V.-H. Winterer<sup>l</sup>, T. Wlodek<sup>z</sup>, S. Wotton<sup>o</sup>, T.R. Wyatt<sup>c</sup>, R. Yaari<sup>z</sup>, G. Yekutieli<sup>z</sup>, M. Yurko<sup>i</sup>, W. Zeuner<sup>r</sup> and G.T. Zorn<sup>j</sup>

<sup>a</sup> Brunel University, Uxbridge, Middlesex UB8 3PH, UK

<sup>b</sup> Department of Physics and Astronomy, Tel Aviv University, Tel Aviv 69978, Israel

<sup>c</sup> Department of Physics, Schuster Laboratory, The University, Manchester M13 9PL, UK

<sup>d</sup> Cavendish Laboratory, Cambridge CB3 0HE, UK

<sup>e</sup> Enrico Fermi Institute and Department of Physics, University of Chicago, Chicago, IL 60637, USA

<sup>f</sup> Dipartimento di Fisica dell' Università di Bologna and INFN, I-40126 Bologna, Italy

<sup>g</sup> Department of Physics, University of Victoria, P.O. Box 3055, Victoria, BC, Canada V8W 3P6

<sup>h</sup> Department of Physics, University of British Columbia, 6224 Agriculture Road, Vancouver, BC, Canada V6T 1Z1

<sup>i</sup> Laboratoire de Physique Nucléaire, Université de Montréal, Montreal, Quebec, Canada H3C 3J7

<sup>j</sup> Department of Physics and Astronomy, University of Maryland, College Park, MD 20742, USA

<sup>k</sup> Queen Mary and Westfield College, University of London, London E1 4NS, UK

<sup>l</sup> Fakultät für Physik, Albert Ludwigs Universität, W-7800 Freiburg, FRG

<sup>m</sup> Universität Hamburg/DESY, II. Institut für Experimental Physik, W-2000 Hamburg 52, FRG

<sup>n</sup> Rutherford Appleton Laboratory, Chilton, Didcot, Oxfordshire OX11 0QX, UK

<sup>o</sup> Physikalisches Institut, Universität Heidelberg, W-6900 Heidelberg, FRG

<sup>p</sup> Physikalisches Institut, Universität Bonn, W-5300 Bonn 1, FRG

<sup>q</sup> School of Physics and Space Research, University of Birmingham, Birmingham B15 2TT, UK

<sup>r</sup> CERN, European Organisation for Particle Physics, CH-1211 Geneva 23, Switzerland

<sup>s</sup> Department of Physics, Carleton University, Colonel By Drive, Ottawa, Ontario, Canada K1S 5B6

<sup>t</sup> University College London, London WC1E 6BT, UK

<sup>u</sup> Department of Physics, Technion-Israel Institute of Technology, Haifa 32000, Israel

<sup>v</sup> Birkbeck College, London WC1E 7HV, UK

<sup>w</sup> Department of Physics, University of California, Riverside, CA 92521, USA

<sup>x</sup> Centre for Research in Particle Physics, Carleton University, Ottawa, Ontario, Canada K1S 5B6

<sup>y</sup> Department of Physics, Indiana University, Swain Hall West 117, Bloomington, IN 47405, USA

<sup>z</sup> Nuclear Physics Department, Weizmann Institute of Science, Rehovot 76100, Israel

<sup>aa</sup> International Centre for Elementary Particle Physics and Department of Physics,

University of Tokyo, Tokyo 113, Japan

and Kobe University, Kobe 657, Japan

<sup>ab</sup> DPPE, CEN-Saclay, F-91191 Gif-sur-Yvette, France

Received 5 May 1992

The inclusive branching ratios of the  $\tau$  lepton to one, three and five charged particle final states are measured from data collected with the OPAL detector at LEP. The data sample consists of 12 707  $e^+e^- \rightarrow \tau^+\tau^-$  candidate events and has an estimated background of 1.9%. The branching ratios are obtained from a simultaneous fit to the data which gives  $B_1 = 84.48 \pm 0.27$  (stat)  $\pm 0.23$  (sys)%,  $B_3 = 15.26 \pm 0.26 \pm 0.22\%$  and  $B_5 = 0.26 \pm 0.06 \pm 0.05\%$  respectively, where  $B_1 + B_3 + B_5$  is constrained to equal one. The inclusive one-prong branching ratio is found to be significantly lower than the 1990 Particle Data Group world average value while the branching ratio to three charged particles is correspondingly higher. The five-prong branching ratio is in agreement with the world average measurement.

## 1. Introduction

This letter reports on the measurement of the inclusive branching ratios of the  $\tau$  lepton to final states containing one, three and five charged particles (1-, 3- and 5-prong decays). It is based on a high statistics sample of  $e^+e^- \rightarrow \tau^+\tau^-$  events collected using the OPAL detector, at centre-of-mass energies between 88.2 and 94.2 GeV, during the 1990 and 1991 LEP running periods. At these energies it is possible to obtain an extremely clean sample of  $\tau$  decays with minimal bias against any particular decay mode. This, combined with the good tracking and particle identification capabilities of the OPAL detector, makes possible a precise measurement of the topological branching ratios of the  $\tau$  lepton.

The main interest in this measurement stems from the so-called "missing decay mode" problem. Previous measurements of  $\tau$  decays [1] suggest an inconsistency between the inclusive 1-prong branching ratio ( $86.1 \pm 0.3\%$ ) and the sum of the 1-prong exclusive branching ratios ( $< 80.2 \pm 1.4\%$  where theoretical constraints are used to limit poorly measured channels) [2,3]. The discrepancy, as determined using this technique, is not entirely resolved by averaging more recent branching ratio measurements [4–6]. However, evidence against such a "missing decay mode" is provided in analyses of all known exclusive decay modes performed by CELLO [8] and ALEPH [4]. ALEPH, for example, set a limit on the branching ratio of new photonic decays to be less than 3.4% at 95% CL. Discrepancies also exist between the

measurements of the inclusive branching ratios. For example, the HRS Collaboration measures an inclusive 1-prong branching ratio of  $86.4 \pm 0.3 \pm 0.3\%$  [7] while the CELLO Collaboration reports a value of  $84.9 \pm 0.4 \pm 0.3\%$  [8].

## 2. The OPAL detector

The OPAL detector is a large general-purpose detector covering almost the entire solid angle [9]. A coordinate system is defined such that the  $z$  axis is along the  $e^-$  beam direction and  $\theta$  is the polar angle. Central tracking chambers, located in a 0.435 T solenoidal magnetic field, measure the momenta of charged particles. The central detector consists of three sets of drift chambers: a high precision vertex chamber, a large-volume jet chamber and "z-chambers" which give a precise  $z$  measurement in the barrel region. The jet chamber is divided into 24 azimuthal sectors each containing 159 sense wires. The measurement of the charge deposition in the jet chamber provides particle identification using  $dE/dx$  information. A barrel time-of-flight (TOF) counter array surrounds the coil in the region  $|\cos\theta| < 0.82$ , which is in turn surrounded by an electromagnetic calorimeter (ECAL) with a presampler. The ECAL consists of a barrel part, covering the region  $|\cos\theta| < 0.82$ , which contains 9440 lead-glass blocks pointing towards the interaction region, and two endcaps covering the region  $0.81 < |\cos\theta| < 0.98$ , consisting of 2264 lead-glass blocks parallel to the beam direction. The amount of material in front of the ECAL in the region  $|\cos\theta| < 0.7$  is approximately  $2X_0/\sin\theta$  (where  $X_0$  is one radiation length). The magnet return yoke is instrumented with nine layers of streamer tubes which serve as a hadron calorimeter (HCAL) and muon tracker. On the outside of the detector four layers of (MUON) drift chambers are used for muon detection. The luminosity is measured using small-angle Bhabha scattering with two forward detector calorimeters between 40 and 120 mrad from the beam direction.

Between the end of the 1990 run and the start of the 1991 run the original (7.8 cm radius) beam pipe was removed and a new beam pipe and silicon microvertex detector were installed inside the existing vertex chamber. While the microvertex detector is not used in this analysis it did introduce some additional ma-

<sup>1</sup> Also at TRIUMF, Vancouver, Canada V6T 2A3.

<sup>2</sup> Present address: Meiji Gakuin University, Yokohama 244, Japan.

<sup>3</sup> Present address: Tel Aviv University, Israel.

<sup>4</sup> Present address: Centre de Physique des Particules de Marseille, Faculté des Sciences de Luminy, Marseille, France.

<sup>5</sup> On leave from Birmingham University, Birmingham B15 2TT, UK.

<sup>6</sup> Present address: Dipartimento di Fisica, Università della Calabria and INFN, 87036 Rende, Italy.

<sup>7</sup> And IPP, McGill University, High Energy Physics Department, 3600 University Str, Montreal, Quebec, Canada H3A 2T8.

<sup>8</sup> Present address: Dept of Physics, University of Oregon, Eugene, Oregon 97405, USA.

<sup>9</sup> Also at Shinshu University, Matsumoto 390, Japan.

terial. This leads to an increased number of photon conversions within the central detector in the 1991 data, compared to the 1990 data sample.

The momentum resolution of the tracking chambers is measured to be  $\Delta p/p \approx 6.8\%$  for  $p_{\perp} = 45$  GeV from  $e^+e^- \rightarrow \mu^+\mu^-$  events, where  $p_{\perp}$  is the momentum transverse to the beam. In the barrel region the ECAL gives an energy resolution of  $\Delta E/E \approx 3\%$  for  $E \approx 45$  GeV from  $e^+e^- \rightarrow e^+e^-$  events. The optimum  $dE/dx$  performance of the jet chamber is  $\sigma_{dE/dx} = 0.030(dE/dx)$  if 159 points are measured on an isolated track. For Monte Carlo studies the OPAL detector response is simulated by a program [10] which treats in detail the detector geometry and material as well as effects of detector resolutions and efficiencies.

### 3. Selection of $e^+e^- \rightarrow \tau^+\tau^-$ events

The procedure used to select  $\tau$  pair events is very similar to that described in previous OPAL publications [11,12]. The distinctive signature of a  $\tau$  pair event is two almost back-to-back jets of one or more charged particles, often accompanied by neutral hadrons or photons. Each jet is accompanied by "missing energy" from the production of one or more neutrinos.

There are four main backgrounds to consider. The first two are  $e^+e^- \rightarrow e^+e^-$  and  $e^+e^- \rightarrow \mu^+\mu^-$  events, which can be identified by the presence of two very high-momentum, back-to-back charged particles with the full centre-of-mass energy,  $E_{CM}$ , deposited in the electromagnetic calorimeter for  $e^+e^- \rightarrow e^+e^-$  and with very little ECAL energy for  $e^+e^- \rightarrow \mu^+\mu^-$ . Hermeticity of the calorimeter ensures correct identification of  $e^+e^- \rightarrow e^+e^-\gamma$  and  $e^+e^- \rightarrow \mu^+\mu^-\gamma$  events which have been a troublesome background for some previous experiments. A third background to  $e^+e^- \rightarrow \tau^+\tau^-$  events comes from  $e^+e^- \rightarrow q\bar{q}$  (multihadronic) events. This background is less significant at LEP than at lower-energy experiments because the particle multiplicity in  $e^+e^- \rightarrow q\bar{q}$  events increases with  $E_{CM}$ , while for  $\tau$  decays it remains constant. Finally, a fourth background comes from two-photon processes  $e^+e^- \rightarrow (e^+e^-)X$  where the final-state electron and positron escape undetected at low angles and the system  $X$  is misidentified as a low-visible-energy  $\tau$  pair event. The contribution to the background from these

processes is small because they lack the enhancement to the cross-section from the  $Z^0$  resonance and because the visible energy of the two-photon system is in general much smaller than that from a  $\tau$  pair event.

Other potential backgrounds arising from cosmic rays and single-beam interactions can be suppressed with straightforward requirements on TOF, on the location of the primary event vertex and on event topology. The consequence of the naturally reduced backgrounds to  $e^+e^- \rightarrow \tau^+\tau^-$  at LEP is that high purity can be attained without sacrificing selection efficiency or strongly biasing for or against certain  $\tau$  decay modes. This substantially reduces the systematic uncertainties in the branching ratio measurements introduced by the event selection.

In selecting  $\tau$  pair events only "good" charged tracks and electromagnetic clusters are considered. In this analysis, a good charged track must have  $p_{\perp} > 100$  MeV, a measured  $|d_0| < 2$  cm, and a measured  $|z_0| < 75$  cm, where  $|d_0|$  is the distance of closest approach of the track to the beam axis, and  $|z_0|$  is the displacement along the beam axis from the nominal interaction point at the point of closest approach to the beam. The track must also have at least 20 measured space points (hits) in the jet chamber. In the barrel, a good ECAL cluster, which is a group of one or more contiguous lead-glass blocks, must have a minimum energy of 100 MeV. In the endcap, the minimum cluster energy is 200 MeV, and the shower cluster must contain at least two lead-glass blocks, no one of which may contribute more than 99% to the cluster's energy.

So as to minimise the bias against 1-5 and 3-3 topology events<sup>#1</sup> somewhat looser cuts are used to eliminate multihadrons than in the general  $\tau$  pair selection. The number of good charged tracks must be in the range from two to eight and the sum of the number of good charged tracks and the number of good ECAL clusters must be less than 18. The cosmic ray background is removed by requiring that there be at least one good charged track with a measured  $|d_0| < 0.5$  cm and a measured  $|z_0| < 20$  cm and requiring that the magnitude of the average  $z_0$  of all good tracks be less than 20 cm. In addition, the TOF must give a signal

<sup>#1</sup> An event with  $i$  charged tracks in one hemisphere and  $j$  charged tracks in the opposite hemisphere is referred to as having an  $i$ - $j$  topology.

consistent with that of an event originating from an  $e^+e^-$  collision.

For this analysis, it is convenient to treat each  $\tau$  decay as a jet, as defined in ref. [11], where charged tracks and ECAL clusters are assigned to cones of half-angle  $35^\circ$ . A  $\tau$  pair candidate must contain exactly two jets, each with at least one charged track and with a total track and cluster energy exceeding 1% of the beam energy. To remove backgrounds from two-photon processes and to remove events with energetic photon radiation, the acolinearity between the two jets must be less than  $15^\circ$ , where the directions of the jets are given by the vector sums of the momenta of the tracks and clusters. The events are restricted to the barrel region of the detector by requiring that the average value of  $|\cos\theta|$  for the two jets satisfy  $|\overline{\cos\theta}| < 0.7$ . This cut is applied in order to eliminate systematic biases introduced by the more severe requirements necessary to reject the  $e^+e^- \rightarrow e^+e^-$  background in the overlap region of the barrel and endcap components of the electromagnetic calorimeter.

Background from  $e^+e^- \rightarrow e^+e^-$  events is eliminated by requirements on the total ECAL energy and the weighted charged track and ECAL energy as for previous OPAL analyses [12]. Events are identified as  $e^+e^- \rightarrow \mu^+\mu^-$  events by the muon pair selection described in ref. [11]; a track in each hemisphere must give a signal consistent with that for a muon in any two out of the ECAL, HCAL or MUON subdetectors and the scalar sum of the charged track momenta plus the energy of the most energetic ECAL cluster must be greater than  $0.6E_{CM}$ . Most of the residual background from  $e^+e^- \rightarrow (e^+e^-)X$  events is rejected by requirements on the total visible energy and the missing transverse momenta as described in ref. [12].

These selection criteria were applied to all the data collected during 1990 and 1991, where the detector components important to the analysis were fully operational, to give a sample of 3794  $\tau$  pair candidate events for the 1990 run and 8913 events for the 1991 run. The data were collected at centre-of-mass energies between 88.2 and 94.2 GeV, with approximately 75% collected on the peak of the  $Z^0$  resonance. From Monte Carlo studies [13] the selection efficiency was estimated to be  $57.1 \pm 0.2\%$ . This corresponds to an efficiency of 92.0% within the  $|\cos\theta| < 0.7$  angular acceptance. The bias introduced by the event selection cuts is given in table 1, the errors on these

Table 1

The acceptance for the different  $\tau$  pair event topologies relative to the overall  $\tau$  pair acceptance.

Event topology	Bias factor
1-1	$0.995 \pm 0.001$
1-3	$1.015 \pm 0.004$
3-3	$0.997 \pm 0.016$
1-5	$0.964 \pm 0.048$

Table 2

Estimated background contaminations in the 12 707  $\tau$  pair candidate events. The errors include both statistical and systematic uncertainties.

Background	Contamination(%)
$e^+e^- \rightarrow q\bar{q}$	$1.0 \pm 0.3$
$e^+e^- \rightarrow e^+e^-$	$0.3 \pm 0.3$
$e^+e^- \rightarrow \mu^+\mu^-$	$0.5 \pm 0.5$
$e^+e^- \rightarrow (e^+e^-)X$	$0.1 \pm 0.1$
total	$1.9 \pm 0.7$

bias factors are dominated by Monte Carlo statistics. The efficiency for selecting events with a 1-3 topology is slightly greater than that for events with a 1-1 topology because of the cuts necessary to eliminate  $e^+e^- \rightarrow e^+e^-$  and  $e^+e^- \rightarrow \mu^+\mu^-$  events. Within the Monte Carlo statistical errors there is no significant bias against events with a 3-3 or 1-5 topology.

Monte Carlo studies of  $e^+e^- \rightarrow e^+e^-$  [14],  $e^+e^- \rightarrow \mu^+\mu^-$  [13],  $e^+e^- \rightarrow q\bar{q}$  [15] and  $e^+e^- \rightarrow (e^+e^-)X$  [16] events give the residual backgrounds shown in table 2. The total background is found to be  $1.9 \pm 0.7\%$  of the total number of events. The main contribution to the systematic uncertainty on the background to events with a 1-1 topology is from muon pair events which are not eliminated by the total energy requirement. The size of this effect is estimated from detailed comparisons of muon pair events with Monte Carlo. For events with topologies other than 1-1 the background is predominantly from multihadrons. In this case an overall systematic uncertainty is obtained by using an algorithm which tags candidate  $\tau$  pair events using only one hemisphere of the event, for events which are identified as multihadrons from the properties of the opposite hemisphere. Assuming that the two hemispheres of the event correspond to two jets which fragment independently, a comparison of the

background estimates from the data and the Monte Carlo is used to derive a systematic uncertainty of  $\pm 25\%$  on the background from multihadrons.

The 11 262 events for which the forward detector was fully operational correspond to a total integrated luminosity of  $17.4 \text{ pb}^{-1}$ . From the estimated acceptance and the measured integrated luminosity [11] and standard model  $\tau$  pair cross-section at each energy point [13], totals of 3730  $\tau$  pair events for the 1990 run and 7307  $\tau$  pair events for the 1991 run are predicted. These predictions are in good agreement with the measured numbers of events after background subtraction (3712 events for the 1990 run and 7336 events for the 1991 run).

#### 4. Measurement of the $\tau$ branching ratios

In this analysis the  $\tau$  topological branching ratios are measured using an unfolding technique. The migration of events from one topology to another caused by tracking inefficiencies, photon conversions and  $K_S^0$  decays are taken into account using the Monte Carlo simulation of the detector [10]. The inclusive 1-, 3- and 5-prong branching ratios are determined from a simultaneous fit to the numbers of events with each measured topology. The additional requirements used to minimise the effects of tracking inefficiencies and the method used to identify tracks originating from photon conversions are described below.

##### 4.1. Track reconstruction effects

Tracks may either be lost or split because of the effects of the track reconstruction. In particular, tracks may be lost in 3-prong or 5-prong  $\tau$  decays where two of the particles are produced with trajectories which overlap within the two hit resolution of the jet chamber, or tracks may be split close to the anode and cathode planes of the jet chamber.

The measured number of jet chamber hits per track for 1, 2, 3 and  $>3$ -prong decays is compared with the Monte Carlo prediction in fig. 1. For a straight, isolated track, in the barrel region of the detector, a maximum of 159 points can be measured. For jets with more than one associated track the measured number of hits per track may be reduced where two tracks overlap, this effect is well described by the Monte

Carlo. For jets with only one associated track, a small excess in the number of tracks with less than 50 hits in the data over the Monte Carlo prediction is visible. Detailed studies show that this effect corresponds to additional split tracks in the data, where part of the track is lost and so the measured number of hits is reduced. Most of these split tracks occur close to the anode and cathode planes of the jet chamber.

For the multiplicity measurement, good charged tracks must have at least 50 jet chamber hits and a momentum greater than 250 MeV (to ensure good electron identification using  $dE/dx$ ). In  $0.14 \pm 0.03\%$  of the  $\tau$  candidates all the charged tracks associated to the jet are eliminated by these cuts (compared to the Monte Carlo prediction of  $0.09 \pm 0.01\%$ ), in this case the multiplicity is assigned to be one.

##### 4.2. Identification of photon conversions

Secondary tracks are produced in the detector from photon conversions and hadronic interactions. Approximately 80% of these are electrons or positrons from photon conversions, where the photons are produced from electromagnetic  $\pi^0$  decays. Secondary electrons are identified using either the  $dE/dx$  measurement alone (which gives a high electron identification efficiency at low momenta, but a reduced efficiency for high momentum electrons because of the poorer  $e-\pi$  separation at high momenta) or a selection which combines looser  $dE/dx$  requirements with the reconstruction of secondary vertices in the central detector (which has an efficiency which is relatively independent of momentum).

The  $dE/dx$  based electron identification uses the difference between the measured  $dE/dx$  and the expected  $dE/dx$  for a pion,  $(dE/dx)^\pi$ , normalised to the error on the  $dE/dx$  measurement,  $\sigma_{dE/dx}$ :

$$\Delta E^\pi = \frac{dE/dx - (dE/dx)^\pi}{\sigma_{dE/dx}}.$$

The quantity  $(dE/dx)^\pi$  is obtained from a parameterization of the  $dE/dx$  distribution as a function of momentum in the  $\tau$  pair data from tracks which are classified as either electrons, muons or pions using criteria similar to those used in the exclusive branching ratio measurement [12] and which are independent of the  $dE/dx$  measurement. This parameterization is also used for the  $dE/dx$  simulation in the Monte

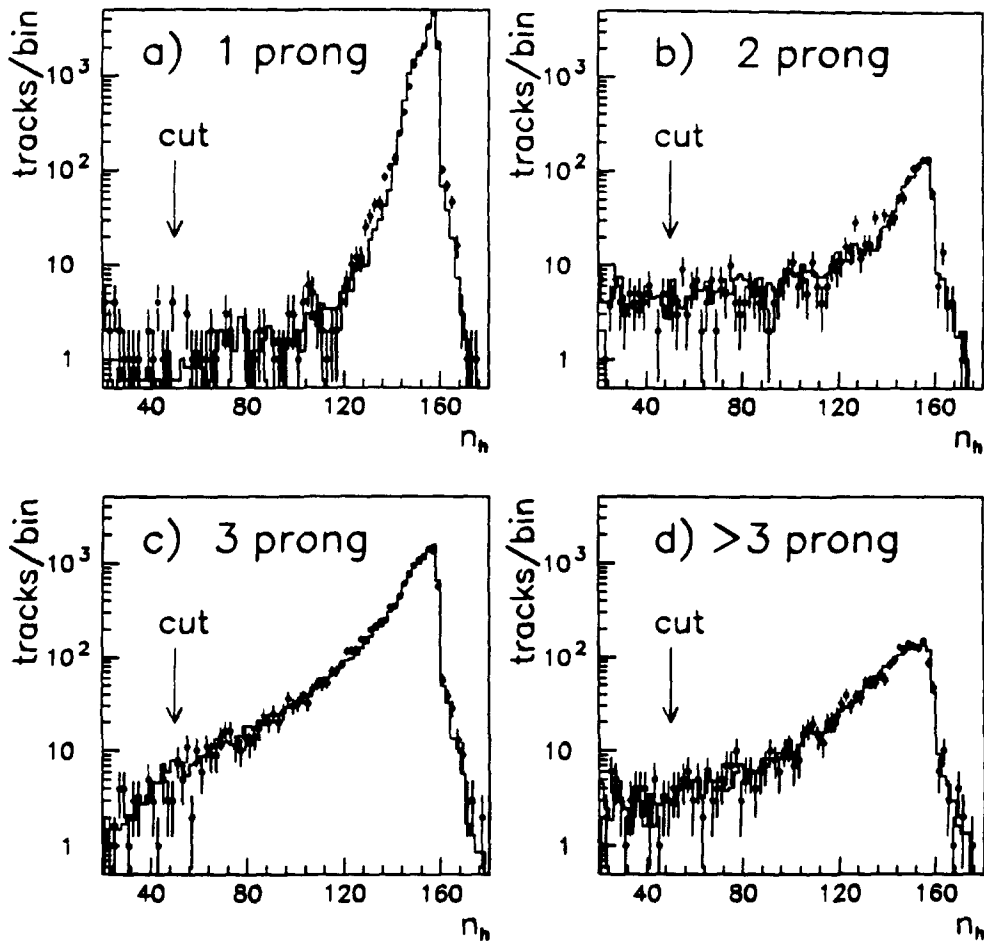


Fig. 1. The number of jet chamber hits per track,  $n_h$ , is plotted for jets with (a) one, (b) two, (c) three and (d) more than three associated charged tracks. The points correspond to the data while the histogram shows the Monte Carlo prediction. The requirement that  $n_h \geq 50$  for "good" charged tracks is shown.

Carlo. In addition to the track quality cuts described above, for the  $dE/dx$  measurement to be used, the number of samples,  $n_h^{dE/dx}$ , must satisfy  $n_h^{dE/dx} \geq 20$ . The  $dE/dx$  resolution is measured to be

$$\sigma_{dE/dx} = \sigma_{\min} \left( \frac{159}{n_h^{dE/dx}} \right)^{0.43} \left( \frac{dE}{dx} \right),$$

where  $\sigma_{\min} = 0.033$  for the 1990 data and  $\sigma_{\min} = 0.034$  for the 1991 data.  $\Delta E^\pi$  is plotted in different momentum regions in fig. 2. A track is classified as an electron if  $\Delta E^\pi > 2.5$ . The second means of identifying photon conversions considers all pairs of oppositely charged tracks, both with  $\Delta E^e > -2$ , where

$$\Delta E^e = \frac{dE/dx - (dE/dx)^e}{\sigma_{dE/dx}}$$

and  $(dE/dx)^e$  is the expected  $dE/dx$  for an electron. At the point of closest approach in the  $xy$  plane, where the tangents of the two tracks are parallel, the tracks must have a separation of less than 0.3 cm in  $xy$  and 50 cm in  $z$ , the cosine of the opening angle between the two tracks must be greater than 0.99 and the cosine of the angle between the vector sum of the momenta of the tracks and the position vector from the origin to the secondary vertex must be greater than 0.996. In addition, the distance from the beam axis to the secondary vertex,  $r_{\text{conv}}$ , must satisfy  $3 < r_{\text{conv}} < 200$  cm,



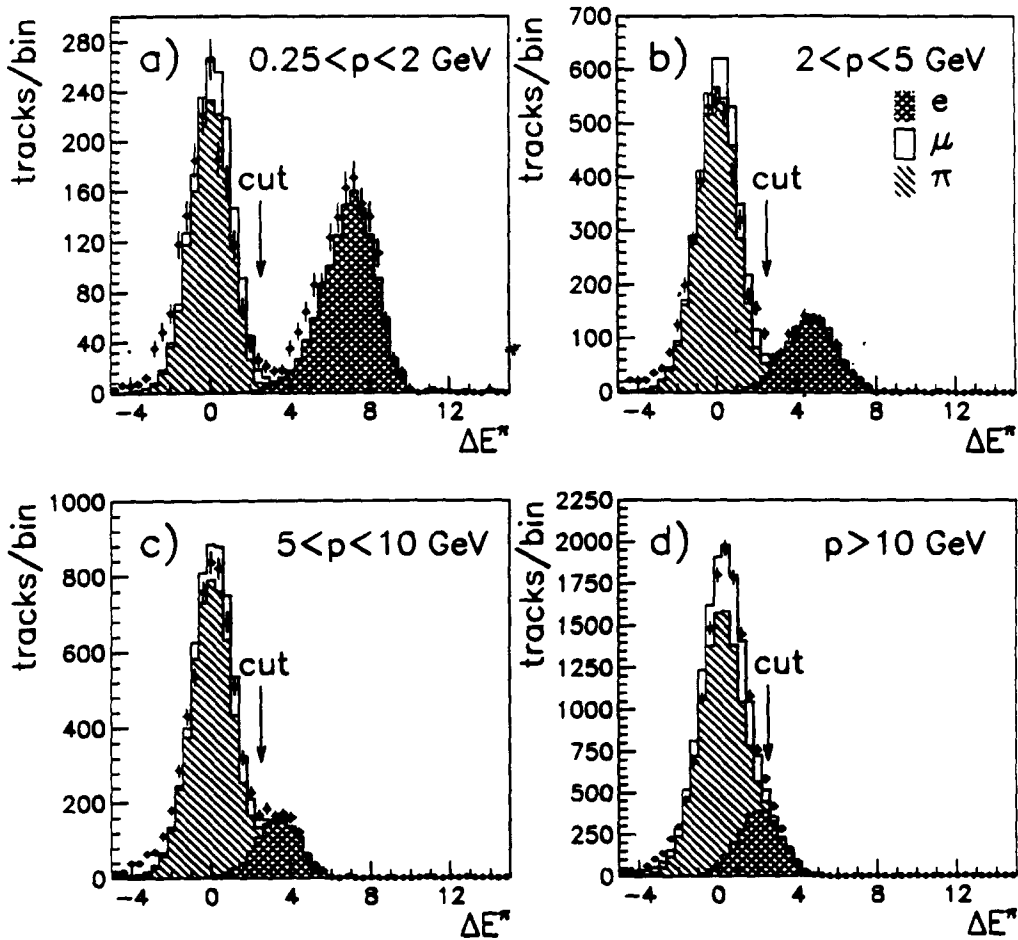


Fig. 2. Distributions of the difference between track energy loss  $dE/dx$  and the expected energy loss for an pion,  $\Delta E^\pi$ , for tracks with 20 or more jet chamber hits used in the  $dE/dx$  measurement and momentum (a) between 0.25 and 2 GeV, (b) between 2 and 5 GeV, (c) between 5 and 10 GeV and (d) above 10 GeV. The points with error bars represent the data while the open histogram shows the Monte Carlo prediction for electrons, muons and pions normalised to the number of  $\tau$  pair events after background subtraction. The cut at  $\Delta E^\pi > 2.5$  used to identify electrons is shown.

the distance from the beam axis to the first hit on either track must be greater than  $r_{\text{conv}} - 20$  cm and the reconstructed photon invariant mass must be less than 0.2 GeV. The radial distribution of identified conversions in data and Monte Carlo for both the 1990 and 1991 detector configurations are shown in fig. 3. The excess in the data compared to the Monte Carlo prediction at  $r_{\text{conv}} = 25$  cm is caused by material known to be missing from the Monte Carlo simulation used for this analysis.

The efficiency for rejecting conversion electrons and

the loss of incorrectly identified pions, as estimated from the Monte Carlo are given in table 3. By identifying electrons using either of the two criteria it is possible to obtain an overall efficiency of order 90% with a minimal loss of pion tracks from 3-prong or 5-prong  $\tau$  decays.

A control sample of 781 visually scanned  $e^+e^- \rightarrow e^+e^-\gamma$  and  $e^+e^- \rightarrow \mu^+\mu^-\gamma$  events, where the radiated photon converts within the central detector to give an  $e^+e^-$  pair, provides an independent check on the efficiency for tagging photon conversions. The measured

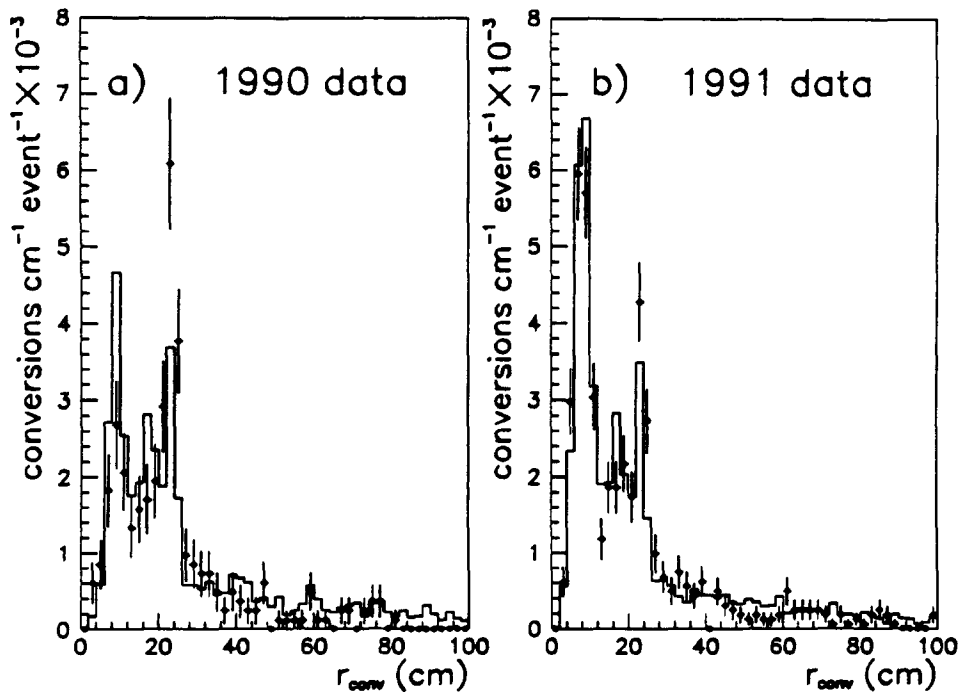


Fig. 3. The distance from the beam axis for reconstructed photon conversions for data taken (a) in 1990 and (b) in 1991. The points represent the data while the open histogram shows the Monte Carlo prediction normalised to the number of  $\tau$  pair events after background subtraction.

efficiency is compared with the Monte Carlo prediction in table 4. Combining the efficiency from events with one additional track with that from events with two additional tracks, both of which are identified as electrons, where these contributions are weighted as in  $\tau$  pair events, gives a discrepancy between data and

Table 3

The efficiency for identifying electrons from photon conversions and loss of pions from  $\tau$  decays using criteria based on either  $dE/dx$  alone, geometrical cuts based on reconstructing secondary vertices or either of the two selections, as estimated from Monte Carlo.

	Conversion electron identification efficiency (%)	Pion misidentification probability (%)
$dE/dx$ cuts	$82 \pm 1$	$0.23 \pm 0.01$
vertex cuts	$67 \pm 1$	$0.23 \pm 0.01$
$dE/dx$ or vertex cuts	$89 \pm 1$	$0.46 \pm 0.02$

Monte Carlo of  $5 \pm 4\%$ . From this a conservative overall systematic uncertainty of  $\pm 10\%$  is assigned to the efficiency for identifying conversion electrons.

The corrected track multiplicity is obtained by subtracting the number of identified electrons from the number of "good" tracks associated to each jet. Since genuine primary electrons may be produced from  $\tau \rightarrow e\nu\bar{\nu}$  decays and in order to minimise the efficiency loss for 3- or 5-prong decays where one pion is incorrectly identified as an electron, the corrected track multiplicity is increased by one if the result after subtraction is an even number (assuming one or more electrons have been found). Since the probability of misidentifying two pions as electrons is small, this is not a significant source of systematic uncertainty on the branching ratio measurement.

#### 4.3. Unfolding the topological branching ratios

The  $\tau$  lepton must decay to an odd number of charged particles, where the branching ratios to

Table 4

Comparison of the efficiency for identifying conversion electrons using a control sample of  $e^+e^- \rightarrow e^+e^-\gamma \rightarrow e^+e^-e^+e^-$  and  $e^+e^- \rightarrow \mu^+\mu^-\gamma \rightarrow \mu^+\mu^-e^+e^-$  events, with predictions from Monte Carlo.

	Number of conversion tracks	Conversion finding efficiency (%)			
		(a) $dE/dx$ cuts	(b) vertex cuts	(a) or (b)	
data	1	$86 \pm 5$	$53 \pm 4$	$89 \pm 5$	} $76 \pm 3$
	2	$55 \pm 4$	$60 \pm 4$	$70 \pm 4$	
Monte Carlo	1	$77 \pm 4$	$53 \pm 3$	$82 \pm 4$	} $81 \pm 3$
	2	$64 \pm 3$	$73 \pm 4$	$81 \pm 4$	

higher charged multiplicities are heavily suppressed; the 5-prong branching ratio is of order 0.1%, while the upper limit on the 7-prong branching ratio is  $B_7 < 0.019\%$  [1]. In practice, however, the measured charged track multiplicity distribution is distorted by errors in the track reconstruction and by secondary tracks produced in the detector from photon conversions and hadronic interactions. To unfold the "true" number of  $\tau$  decays to 1-, 3- and 5-prongs, efficiencies and cross-contaminations between the different event topologies obtained from Monte Carlo simulation are used. Four possible true event topologies are considered here: 1-1, 1-3, 3-3 and 1-5. The corrected number of events in each class,  $N_{kl}$ , is related to the measured number of events with an  $i$ - $j$  topology,  $n_{ij}$ , by

$$n_{ij} - n_{ij}^B = \sum_{kl} \epsilon_{kl \rightarrow ij} f_{kl} N_{kl},$$

where  $n_{ij}^B$  is the estimated non- $\tau$  background,  $f_{kl}$  is the bias introduced by the event selection and  $\epsilon_{kl \rightarrow ij}$  is the probability of a  $\tau$  pair event with a "true"  $k$ - $l$  topology resulting in a measured  $i$ - $j$  topology. The inclusive branching ratios,  $B_1$ ,  $B_3$  and  $B_5$ , are then given by

$$N_{kl} = (2 - \delta_{kl}) B_k B_l N_{\text{tot}},$$

where  $N_{\text{tot}}$  is the total number of  $\tau$  pair events. The branching ratios are obtained from a simultaneous fit to the numbers of events with the topologies listed in table 5. Of the 71 events eliminated by restricting the fit to these topologies  $\approx 58$  correspond to background from  $e^+e^- \rightarrow q\bar{q}$  events. This method has the advantage that it is independent of the integrated luminosity measurement and the overall efficiency of the  $\tau$  pair selection and so gives a smaller systematic error on the branching ratio measurement than if the absolute

number of events in each topology were used.

The  $\epsilon$  matrix which describes the efficiency and cross-contamination between decay modes is given in table 6. The additional material introduced with the microvertex detector necessitates treating the 1990 and 1991 data separately. The most important contributions to the off-diagonal elements of the  $\epsilon$  matrix are from the track reconstruction and from secondary tracks produced in the detector, as described below:

- The merging of overlapping tracks is the dominant contribution to  $\epsilon_{13 \rightarrow 11}$ ,  $\epsilon_{13 \rightarrow 12}$ ,  $\epsilon_{15 \rightarrow 13}$ ,  $\epsilon_{15 \rightarrow 14}$ ,  $\epsilon_{33 \rightarrow 13}$  and  $\epsilon_{33 \rightarrow 23}$ . Comparing the number of events with a 1-2 topology between data and Monte Carlo (over 60% of which have a "true" 1-3 topology) reveals an excess of  $17 \pm 9\%$  in the Monte Carlo. From this a conservative systematic error of  $\pm 25\%$  is assigned to these elements of the  $\epsilon$  matrix.

- Secondary tracks from photon conversions and hadronic interactions are the dominant contribution to  $\epsilon_{11 \rightarrow 12}$ ,  $\epsilon_{11 \rightarrow 13}$ ,  $\epsilon_{13 \rightarrow 23}$ ,  $\epsilon_{13 \rightarrow 33}$ ,  $\epsilon_{13 \rightarrow 14}$  and  $\epsilon_{13 \rightarrow 15}$ . Three potential sources of systematic error on these quantities are considered. Firstly, the discrepancy shown in fig. 3 was investigated by generating additional Monte Carlo events with a corrected material distribution and re-evaluating the  $\epsilon$  matrix. This gives a systematic error on these quantities of  $\pm 13\%$ . Secondly, the effect of the systematic error on the efficiency for identifying photon conversions was estimated by varying the conversion finding efficiency in the Monte Carlo by  $\pm 10\%$ . This leads to an additional  $\pm 7\%$  systematic uncertainty on these elements of the  $\epsilon$  matrix. Finally, if the number of  $\pi^0$ s per  $\tau$  decay is not correctly modelled by the Monte Carlo this may bias the result. The main source of uncertainty is the relatively poorly measured  $\tau \rightarrow \pi^+ 3\pi^0 \nu$  branching fraction. Varying this between 0 and 5%

Table 5

The measured number of events with each topology,  $n_{ij}$ , the estimated distribution for the background,  $n_{ij}^B$ , and the predicted number of events in each topology from the Monte Carlo using the fitted branching ratios,  $n_{ij}^{\text{fit}} = \sum_{kl} \epsilon_{kl \rightarrow ij} f_{kl} N_{kl}$ .

$i-j$	1990 data			1991 data		
	$n_{ij}$	$n_{ij}^B$	$n_{ij}^{\text{fit}}$	$n_{ij}$	$n_{ij}^B$	$n_{ij}^{\text{fit}}$
1-1	2663	$34.2 \pm 22.8$	$2618.3 \pm 19.2 \pm 7.4$	6094	$80.2 \pm 53.5$	$5994.9 \pm 30.5 \pm 23.9$
1-2	65	$1.0 \pm 0.7$	$55.8 \pm 2.8 \pm 9.2$	144	$2.3 \pm 1.6$	$166.3 \pm 5.2 \pm 28.2$
1-3	901	$1.5 \pm 0.9$	$927.5 \pm 11.4 \pm 10.7$	2247	$3.5 \pm 2.0$	$2248.3 \pm 19.6 \pm 34.3$
1-4	12	$4.4 \pm 1.5$	$8.5 \pm 1.2 \pm 1.0$	41	$10.4 \pm 3.5$	$28.4 \pm 2.3 \pm 3.4$
1-5	22	$3.5 \pm 1.3$	$18.2 \pm 2.0 \pm 1.1$	66	$8.1 \pm 3.1$	$58.3 \pm 3.7 \pm 3.8$
2-2	2	$2.5 \pm 1.1$	$0.1 \pm 0.1 \pm 0.0$	3	$5.8 \pm 2.6$	$0.7 \pm 0.3 \pm 0.0$
2-3	19	$2.0 \pm 1.0$	$8.4 \pm 1.1 \pm 1.2$	36	$4.6 \pm 2.3$	$28.8 \pm 2.3 \pm 4.9$
3-3	98	$5.9 \pm 1.7$	$81.7 \pm 3.3 \pm 1.6$	223	$13.9 \pm 4.0$	$204.8 \pm 6.1 \pm 5.7$
total	3782	$54.8 \pm 23.0$	$3718.4 \pm 22.9 \pm 16.1$	8854	$128.8 \pm 54.0$	$8730.5 \pm 37.4 \pm 51.2$

gives an additional systematic error of  $\pm 9\%$  on  $\epsilon_{11 \rightarrow 12}$  and  $\epsilon_{11 \rightarrow 13}$ .

– There is also a contribution to  $\epsilon_{11 \rightarrow 12}$  and  $\epsilon_{11 \rightarrow 13}$  from  $\tau \rightarrow K^* \nu$  decays, where the  $K^*$  decays via a  $K_S^0$  which subsequently decays as  $K_S^0 \rightarrow \pi^+ \pi^-$ . Since the branching ratio for this process is small ( $\sim 0.5\%$ ) this does not contribute significantly to the systematic error.

The measured number of events and the expected non- $\tau$  background for each topology are given in table 5. The backgrounds from  $e^+e^- \rightarrow e^+e^-$ ,  $e^+e^- \rightarrow \mu^+\mu^-$  and  $e^+e^- \rightarrow (e^+e^-)X$  events nearly all have a 1-1 topology, while the multiplicity distribution for the multihadronic background is taken from the Monte Carlo prediction. The error on the  $e^+e^- \rightarrow e^+e^-$ ,  $e^+e^- \rightarrow \mu^+\mu^-$  and  $e^+e^- \rightarrow (e^+e^-)X$  backgrounds includes both Monte Carlo statistical and systematic errors. The error on the multihadron background is from Monte Carlo statistics only, the overall systematic scale uncertainty is considered below.

A  $\chi^2$  fit to the 1990 data with  $B_1 + B_3 + B_5$  constrained to equal one and with any two out of  $B_1$ ,  $B_3$  and  $B_5$  as free parameters, gives  $B_1 = 85.10 \pm 0.48 \pm 0.17\%$ ,  $B_3 = 14.67 \pm 0.47 \pm 0.16\%$  and  $B_5 = 0.23 \pm 0.10 \pm 0.04\%$  with a  $\chi^2$  of 5.6 for five degrees of freedom. A fit to the 1991 data gives  $B_1 = 84.22 \pm 0.32 \pm 0.20\%$ ,  $B_3 = 15.51 \pm 0.32 \pm 0.20\%$  and  $B_5 = 0.27 \pm 0.08 \pm 0.04\%$  with a  $\chi^2$  of 2.1 for five degrees of freedom. Here, the first error is the combined statistical error from the data and the  $\tau$  pair Monte Carlo and the second error is from the error on the non- $\tau$  background and the systematic errors on the  $\epsilon$

matrix. The Monte Carlo prediction for the number of events in each bin using the fitted branching ratios is given in table 5. The agreement between data and Monte Carlo is good.

There are two further sources of systematic error to be considered. Scaling the hadronic background by  $\pm 25\%$  and re-applying the fit gives an estimate of the uncertainty introduced by the systematic error on the level of the multihadronic background. This gives a contribution to the systematic error on  $B_1$ ,  $B_3$  and  $B_5$  (as a fraction of the total number of  $\tau$  decays) of  $\pm 0.07\%$ ,  $\pm 0.05\%$  and  $\pm 0.023\%$  respectively. The dominant source of systematic error from the event selection is from the cut on the mean jet  $|\cos \theta|$  which is used to define the angular acceptance. Varying this cut between 0.65 and 0.75 and repeating the analysis gives an additional contribution to the systematic error on  $B_1$  and  $B_3$  of 0.1% of the number of  $\tau$  decays. The cuts used to identify muon pair events were varied to estimate the effect on the branching ratio measurement of the systematic errors on the bias factors quoted in table 1. The contribution to the overall systematic error from this source is negligible.

The sources of systematic error on the measurement of  $B_1$ ,  $B_3$  and  $B_5$  are summarised in table 7. Varying the number of jet chamber hits required for a “good” track between 30 and 80 and repeating the analysis provides an additional check on the systematic error introduced by the track reconstruction. This gives a variation in the fitted branching ratios consistent with the systematic error quoted in table 7.

Table 6

The efficiency and cross-contamination between decay modes,  $\epsilon_{kl \rightarrow ij}$ , estimated from Monte Carlo studies for the 1990 and the 1991 detector configuration. The first error is from Monte Carlo statistics, while the second error is from systematic studies described in the text.

	<i>ij</i>	<i>kl</i>			
		1-1	1-3	1-5	3-3
1990 detector	1-1	97.72 ± 0.72 ± 0.27	0.31 ± 0.07 ± 0.08	<1.9	<0.2
	1-2	0.83 ± 0.07 ± 0.14	3.53 ± 0.23 ± 0.88	<1.9	<0.2
	1-3	1.39 ± 0.09 ± 0.24	93.61 ± 1.18 ± 0.91	5.7 ± 3.3 ± 1.4	0.3 ± 0.2 ± 0.1
	1-4	<0.1	0.58 ± 0.09 ± 0.09	17.1 ± 5.7 ± 4.3	<0.2
	1-5	<0.1	0.63 ± 0.10 ± 0.09	76.9 ± 12.1 ± 4.5	<0.2
	2-2	<0.1	<0.1	<1.9	<0.2
	2-3	<0.1	0.41 ± 0.08 ± 0.06	<1.9	5.2 ± 0.9 ± 1.3
	3-3	<0.1	0.81 ± 0.11 ± 0.12	<1.9	92.4 ± 4.0 ± 1.3
1991 detector	1-1	96.82 ± 0.49 ± 0.38	0.38 ± 0.05 ± 0.10	<0.8	<0.1
	1-2	1.00 ± 0.05 ± 0.17	4.52 ± 0.18 ± 1.13	<0.8	<0.1
	1-3	2.03 ± 0.07 ± 0.34	91.68 ± 0.82 ± 1.16	2.3 ± 1.4 ± 0.6	1.0 ± 0.3 ± 0.2
	1-4	<0.1	0.89 ± 0.08 ± 0.13	14.1 ± 3.3 ± 3.5	<0.1
	1-5	<0.1	1.04 ± 0.09 ± 0.16	82.0 ± 8.0 ± 3.6	<0.1
	2-2	<0.1	<0.1	<0.8	<0.1
	2-3	<0.1	0.41 ± 0.06 ± 0.06	<0.8	8.9 ± 0.9 ± 2.2
	3-3	<0.1	0.92 ± 0.08 ± 0.14	<0.8	87.1 ± 2.8 ± 2.2

Table 7

Systematic errors on the measurement of  $B_1$ ,  $B_3$  and  $B_5$  as a fraction of the total number of  $\tau$  decays, for the combined measurement from both 1990 and 1991 data.

	$\Delta B_1$ (%)	$\Delta B_3$ (%)	$\Delta B_5$ (%)
non- $\tau$ background	±0.14	±0.13	±0.035
track reconstruction	±0.12	±0.12	±0.012
$\gamma$ conversions	±0.10	±0.10	±0.027
event selection	±0.10	±0.10	-
total	±0.23	±0.22	±0.046

## 5. Summary and discussion

The inclusive branching ratios of the  $\tau$  lepton to one, three and five charged particle final states are measured to be  $B_1 = 84.48 \pm 0.27$  (stat)  $\pm 0.23$  (sys)%,  $B_3 = 15.26 \pm 0.26 \pm 0.22\%$  and  $B_5 = 0.26 \pm 0.06 \pm 0.05\%$  respectively. These measurements have been obtained from a fit where  $B_1 + B_3 + B_5$  is constrained to equal one. The correlations between the fitted branching ratios are given by the matrix

$$\rho = \begin{pmatrix} 1.0 & -0.97 & -0.15 \\ -0.97 & 1.0 & -0.07 \\ -0.15 & -0.07 & 1.0 \end{pmatrix}.$$

While the measurements of  $B_1$  and  $B_3$  are highly correlated, the measurement of  $B_5$  is relatively independent of  $B_1$  and  $B_3$ .

The measured 5-prong branching ratio is in agreement with the 1990 Particle Data Group world average [1]. However, the measured 1-prong branching ratio is lower than the world average by more than three standard deviations while the 3-prong branching fraction is correspondingly higher than the average value. The errors on these measurements are of comparable size to those on the 1990 world averages. The 1-prong measurement confirms the result obtained by the CELLO Collaboration [8] which also gave a 1-prong branching ratio which was significantly smaller than previous measurements. It is also in agreement with the results obtained by other LEP experiments [4]. The significance of the "missing decay mode" effect as determined by the OPAL 1-prong branching fraction and the sum of average exclusive branching ratios [1] is less than three standard deviations. A four standard deviation effect was reported in reference [1]. While this result is not sufficient by itself to entirely resolve the problem it does go some way towards reducing the size of the effect.

### Acknowledgement

It is a pleasure to thank the SL Division for the efficient operation of the LEP accelerator, and for its continuing close cooperation with our experimental group. In addition to the support staff at our own institutions we are pleased to acknowledge the Department of Energy, USA, National Science Foundation, USA, Science and Engineering Research Council, UK, Natural Sciences and Engineering Research Council, Canada, Israeli Ministry of Science, Minerva Gesellschaft, Japanese Ministry of Education, Science and Culture (the Monbusho) and a grant under the Monbusho International Science Research Program, American Israeli Bi-national Science Foundation, Direction des Sciences de la Matière du Commissariat à l'Énergie Atomique, France, Bundesministerium für Forschung und Technologie, FRG, National Research Council of Canada, Canada, A.P. Sloan Foundation and Junta Nacional de Investigação Científica e Tecnológica, Portugal.

### References

- [1] Particle Data Group, J.J. Hernández et al., Review of particle properties, Phys. Lett. B 239 (1990), pVI.14.
- [2] B.C. Barish and R. Stroynowski, Phys. Rep. 157 (1988) 1.
- [3] T.N. Truong, Phys. Rev. D 30 (1984) 1509; F.J. Gilman and S.H. Rhie, Phys. Rev. D 31 (1985) 1066; K.G. Hayes and M.L. Perl, Phys. Rev. D 38 (1988) 3351.
- [4] ALEPH Collab., D. Decamp et al., CERN-PPE/91-186 (1991), submitted to Z. Phys. C. L3 Collab., B. Adeva et al., Phys. Lett. B 265 (1991) 451.
- [5] ARGUS Collab., H. Albrecht et al., DESY/91-084 (July 1991).
- [6] K. Riles, Proc. Particles and fields 91, Vol. 1, Univ. of British Columbia (Vancouver, August 1991).
- [7] HRS Collab., S. Abachi et al., Phys. Rev. D 40 (1989) 902.
- [8] CELLO Collab., H.J. Behrend et al., Phys. Lett. B 222 (1989) 163; Z. Phys. C 46 (1990) 537.
- [9] OPAL Collab., K. Ahmet et al., Nucl. Instrum. Methods A 305 (1991) 275.
- [10] J. Allison et al., Comput. Phys. Commun. 47 (1987) 55; D. R. Ward, Proc. MC'91 Workshop (NIKHEF, Amsterdam, 1991); J. Allison et al., CERN-PPE/91-234 (1991), to be published in Nucl. Instrum. Methods.
- [11] OPAL Collab., G. Alexander et al., Z. Phys. C 52 (1991) 175.
- [12] OPAL Collab., G. Alexander et al., Phys. Lett. B 266 (1991) 201.
- [13] S. Jadach, J.H. Kuhn and Z. Was, Comput. Phys. Commun. 64 (1991) 275; TAUOLA; S. Jadach, B.F.L. Ward and Z. Was, Comput. Phys. Commun. 66 (1991) 276; KORALZ, Version 3.7.
- [14] M. Böhm, A. Denner and W. Hollik, Nucl. Phys. B 304 (1988) 687; F.A. Berends, R. Kleiss and W. Hollik, Nucl. Phys. B 304 (1988) 712; BABAMC.
- [15] T. Sjöstrand, Comput. Phys. Commun. 39 (1986) 347; JETSET.
- [16] R. Bhattacharya, J. Smith and G. Grammer, Phys. Rev. D 15 (1977) 3267; J. Smith, J.A.M. Vermaseren and G. Grammer, Phys. Rev. D 15 (1977) 3280.